

Evaluation of a multi-frame blind deconvolution algorithm using Cramér-Rao bounds

Charles C. Beckner, Jr.

*Air Force Research Laboratory, 3550 Aberdeen Ave SE, Kirtland AFB, New Mexico, USA
87117-5776*

Charles L. Matson

*Air Force Research Laboratory, 3550 Aberdeen Ave SE, Kirtland AFB, New Mexico, USA
87117-5776*

Abstract: Sample statistics from a multi-frame blind-deconvolution (MFBD) algorithm are compared with Cramer-Rao bounds (CRB) in order to evaluate the noise reduction performance of the MFBD algorithm. In this paper, CRB theory is employed as a metric to evaluate the performance of a MFBD imaging algorithm developed at the Air Force Maui Optical and Supercomputing Site, a site operated by the Air Force Research Laboratory. Sample variances from the MFBD algorithm named PCID (physically constrained blind deconvolution) and CRB lower bounds to variances are compared for a baseline model imaging scenario that employs an object, blurring, photon noise and read noise. The variance reduction effects produced by imposing support constraints on the object and on the point spread function (PSF) are analyzed. Pixel-by-pixel sample variance maps are compared to CRB maps for the case of perfect and loose object support constraints. The PCID sample variance maps are evaluated against CRBs both to determine the relative magnitude of these variances as opposed to CRB lower bounds and to assess overall morphology differences. For the baseline model imaging scenario, the PCID pixel-by-pixel sample variance magnitudes match their associated CRBs, and the PCID sample variances and CRBs share the same overall morphology. Additionally, PCID sample variance results are presented for cases where the baseline model imaging and post-processing scenario above is extended beyond where CRB theory has been developed. The model imaging scenario is extended to include the use of positivity in the imaging algorithm.

1. Introduction

Recently, Cramér-Rao bound (CRB) theory for support-constrained multi-frame blind deconvolution was developed.¹ CRB theory can be used to generate algorithm-independent lower bounds to either unbiased or biased estimators of a set of parameters. In this paper, the CRB theory for unbiased estimators is employed as a metric to evaluate the performance of a multi-frame blind-deconvolution (MFBD) imaging algorithm developed at the Air Force Maui Optical and Supercomputing Site, a site operated by the Air Force Research Laboratory. Sample variances from our MFBD algorithm named PCID (Physically Constrained Blind Deconvolution) are compared to their corresponding CRBs for a model imaging scenario. PCID employs a conjugate gradient search algorithm in order to minimize a cost function that expresses the difference between the given measurement and estimates of the measurement based on convolving the estimated object and blurring point spread functions (PSF). It is shown that the PCID sample variances and the CRBs have similar morphology, and that the PCID sample variances approach their respective CRBs, i.e., they nearly achieve the theoretical performance bounds of noise reduction.

Then, the imaging scenarios employed in the PCID/CRB comparison are once again post-processed using PCID, this time enforcing a positivity constraint. The associated positivity constrained CRBs are not presented. The positivity enforced PCID results are evaluated against the unconstrained PCID and CRB results both to determine the numerical effect of positivity on reconstructions and to assess morphological differences. The remainder of this paper is structured as follows: the basic imaging model and an explanation of the PCID algorithm are given in Section 2, a brief explanation of how Cramer-Rao bound theory is employed in this research is provided in Section 3, results are presented in Section 4, then a conclusion and remarks about future work are given in Section 5.

2. Imaging model and PCID

The imaging model used in this research is

$$i_m(\mathbf{x}) = o(\mathbf{x}) * h_m(\mathbf{x}) + n_m(\mathbf{x}) \quad (1)$$

where i_m is the m^{th} measured image, \mathbf{x} specifies locations in the image, $*$ denotes convolution, h_m is the m^{th} PSF, o is the object, and n_m is the m^{th} zero mean, spatially-uncorrelated noise function. In a typical imaging application, the exposure time of $i_m(\mathbf{x})$ is on the order of 1-10 ms so that high frequency content out to the diffraction limit is retained.² Then, our PCID algorithm can be employed to extract much of the information content concealed by the blurring and noise. The PCID algorithm jointly estimates both the object and the blurring function from the blurred and noisy image data by minimizing the following cost function:

$$J(\hat{o}, \hat{h}_1, \dots, \hat{h}_M) = \sum_m \sum_{\mathbf{x}} [\hat{i}_m(\mathbf{x}) - i_m(\mathbf{x})]^2 \quad (2)$$

where $J(\dots)$ is the cost function to be minimized with respect to estimates of the object and all the PSFs, using all M measured images, and the $\hat{i}_m(\mathbf{x})$ are the estimates of the M images generated by convolving the estimated object and the M blurring functions.³ It should be noted that both positivity and support constraints can be imposed on the algorithm.

3. Cramer-Rao Bounds

Cramer-Rao bound theory provides an algorithm-independent analysis approach to explore how the combination of the model imaging scenario and support constraints impact reconstructed image quality. This approach is employed because it produces “gold standard” results that characterize the benefits of prior knowledge constraints without the concerns that the results are algorithm dependent and that the results may change if a more clever algorithm is employed. Cramér-Rao lower bound (CRB) theory relies upon the Fisher information matrix (FIM) to generate lower bounds to the variances of any estimate of a collection of random variables. As a result, it can be viewed as characterizing how the information content in a prior knowledge constraint reduces noise in an image, rather than how a specific algorithm uses the information in a prior knowledge constraint to reduce noise.⁴

4. Results

The measured data consisted of the satellite object shown in Fig.1 convolved with M atmospheric blurring point spread functions corresponding to $D/r_0 = 8$ and corrupted by either zero-mean Gaussian white noise or by Poisson distributed photon noise and zero-mean Gaussian white noise (read noise), where D is the telescope diameter and r_0 is the Fried parameter. The PSFs were made invertible by first low-pass-filtering them with a square low-pass filter and then embedding these low-pass-filtered versions in an array of the same size as the low-pass filter. They were then made to have finite support by applying a circular support constraint in the image domain. These modifications to the PSFs were made to simplify the comparison between sample variances and CRBs by making possible unbiased estimates of the object. A large set of blurred and noisy data was generated using this approach for use in PCID reconstructions. Pixel-by-pixel sample variances were produced from support-constrained PCID restorations using this dataset with $M = 10$. In this paper, perfect object support where the support boundary conforms perfectly to the ocnr object, and the blur2 and circular object support shown in Fig. 1 were employed in PCID restorations. CRBs for this imaging situation were obtained from previous work.⁵

CRB, PCID, and PCID with positivity enforced results for the read noise only case are presented in Figure 2. These results are depicted as pixel-by-pixel variance maps, normalized to the highest valued pixel of the associated CRB variance map. PCID sample variances and CRBs, for the case of perfect object support, tight but non-perfect blur2 object support, and circular support are shown. The CRB and PCID results were generated from the same imaging scenario, so that the CRBs can be employed as a metric to evaluate the PCID results. The similarities in morphology show that the CRBs and the PCID sample variances are in qualitative agreement for all three support constraints sizes. Also, the numerical value of the summed CRB arrays and PCID sample variance arrays shows

that PCID is approaching the theoretical limits to noise reduction for this imaging scenario, as given in Table 1. The mean-square error (MSE), i.e., the total variance summed with the total squared bias (these results were largely unbiased), of the PCID reconstructions nearly meet the CRBs.⁶ In order to achieve the CRBs, the PCID algorithm must drive to the global minimum solution of the given noise corrupted, blind deconvolution problem. In imaging situations where positivity was not employed, the blurred and noisy data could be used to seed the PCID algorithm. In challenging imaging situations where the object support is significantly larger than the object and where positivity is employed, the PCID algorithm can get stuck in local minima. In this case, the initial object guess employed to seed the algorithm consisted of the ocnr object with noise that amounted to three or more times its associated CRB variance.

The summed sample variances of the positivity constrained case are the same or lower than the unconstrained case. Although the positivity constrained CRBs are not provided, it seems reasonable to conclude that the variances in the positivity constrained case are lower because negative intensity values are eliminated thereby reducing the range of possible variance from the mean. Also, the squared bias of the reconstructions rose above the unconstrained PCID sample variance levels as might be expected from the application of the positivity constraint. Also, positivity appears to operate like an object support constraint when the applied object support constraint is loose, as shown in the positivity enforced, circular support constrained results in Figure 2.

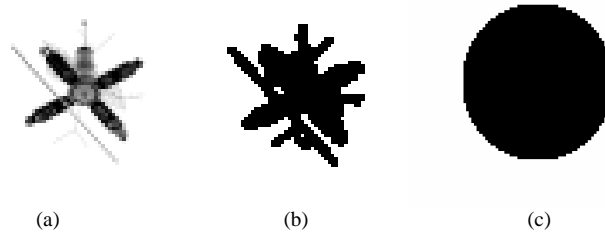


Fig. 1. (a) Computer-simulated satellite model, (b) the blur2 support constraint and (c) circular support used for the PCID and CRB calculation.

Totals within support constraint:	true support	blur2 support	circular support
CRBs	4.8×10^5	7.7×10^5	3.1×10^6
PCID	4.9×10^5	8.0×10^5	3.8×10^6
PCID <i>positivity enforced</i>	4.9×10^5	5.5×10^5	5.8×10^5

Table 1. Read noise case. The total CRBs within a support constraint consist of the summation of all the minimum possible pixel-by-pixel variances that any unbiased estimate could achieve. For each PCID result presented in this table, the summed pixel-by-pixel sample variances were drawn from a set of fifty reconstructions. Each reconstruction was post-processed from measurements formed from the ocnr object, the ten PSFs, and independent read noise realizations.

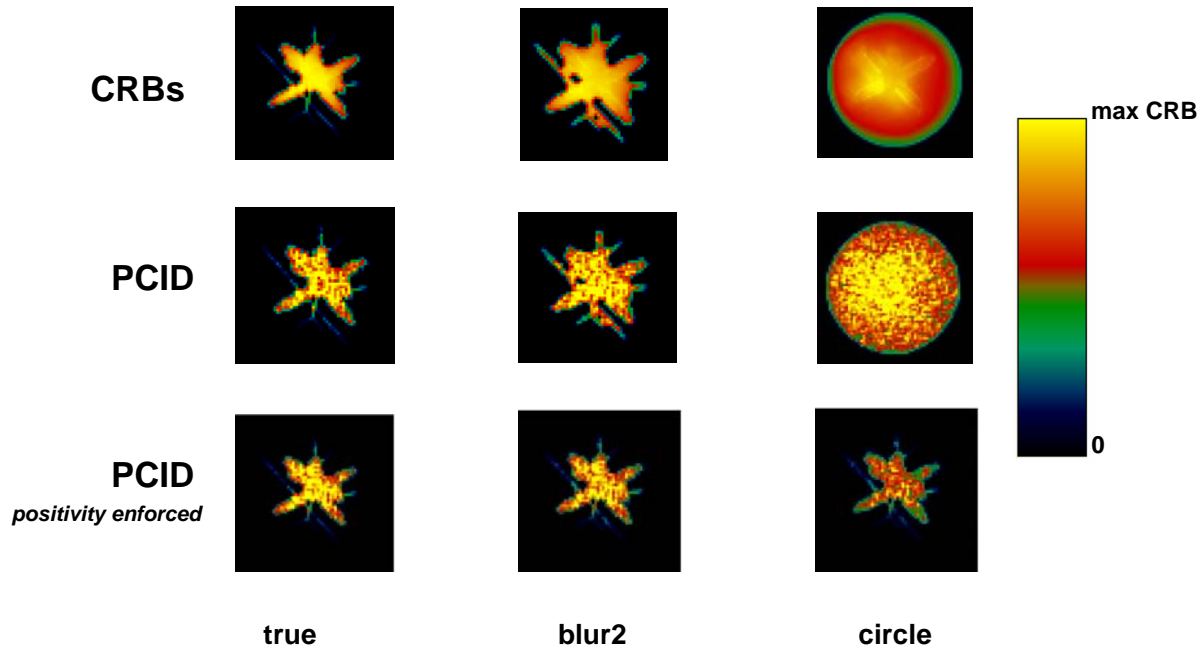


Fig. 2. Read noise only case. The first row consists of pixel-by-pixel CRB lower bounds to variance maps. The second and third row consist of PCID sample variance maps and for unconstrained and positivity constrained cases. Support constrained cases are organized by column: perfect or true support, blur2 non-perfect support, and circular support. All PCID variance maps are normalized to the highest value within the associated CRB map located at the top of the column.

CRB, PCID, and PCID with positivity enforced results for the photon and read noise are presented in Figure 3. As in the read noise only case, these results are depicted as pixel-by-pixel variance maps, normalized to the highest valued pixel of the associated CRB variance map. PCID sample variances and CRBs, for the case of perfect object support, tight but non-perfect blur2 object support, and circular support are shown. The CRB and PCID results were generated from the same imaging scenario, so that the CRBs can be employed as a metric to evaluate the PCID results. Again, the similarities in morphology between the two maps show that the CRBs and the PCID sample variances are in qualitative agreement. Also, the numerical value of the summed CRB arrays and PCID sample variance arrays shows that PCID is approaching the theoretical limits to noise reduction for this imaging scenario, as given in Table 2. The MSE of the PCID reconstructions nearly meet the CRBs.⁶ It is worth noting that the MSE was almost entirely comprised of variance; these results were largely unbiased.

In order to achieve the CRBs, the PCID algorithm must drive to the global minimum solution of the given noise corrupted, blind deconvolution problem. In imaging situations where positivity was not employed, the blurred and noisy measurement data could be used to seed the PCID algorithm. In challenging imaging situations where the object support is significantly larger than the object and where positivity is employed, the PCID algorithm can get stuck in local minima, e.g., the positivity constrained case with circular support, shown at the bottom right in Figure 3, did not converge to the global minimum. In this case, the initial object guess employed to seed the algorithm consisted of the ocnr object with noise that amounted to three or more times its associated CRB variance.

Totals within support constraint:	true support	blur2 support	circular support
CRBs	2.0×10^{10}	2.4×10^{10}	2.8×10^{10}
PCID	2.3×10^{10}	2.7×10^{10}	3.0×10^{10}
PCID <i>positivity enforced</i>	2.2×10^{10}	2.3×10^{10}	Not available

Table 2. Photon and read noise case. The total CRBs within a support constraint consist of the summation of all the minimum possible pixel-by-pixel variances that any unbiased estimate could achieve. For each PCID result presented in this table, the summed pixel-by-pixel sample variances were drawn from a set of fifty reconstructions. Each reconstruction was post-processed from measurements formed from the ocnr object, the ten PSFs, and independent photon noise and read noise realizations.

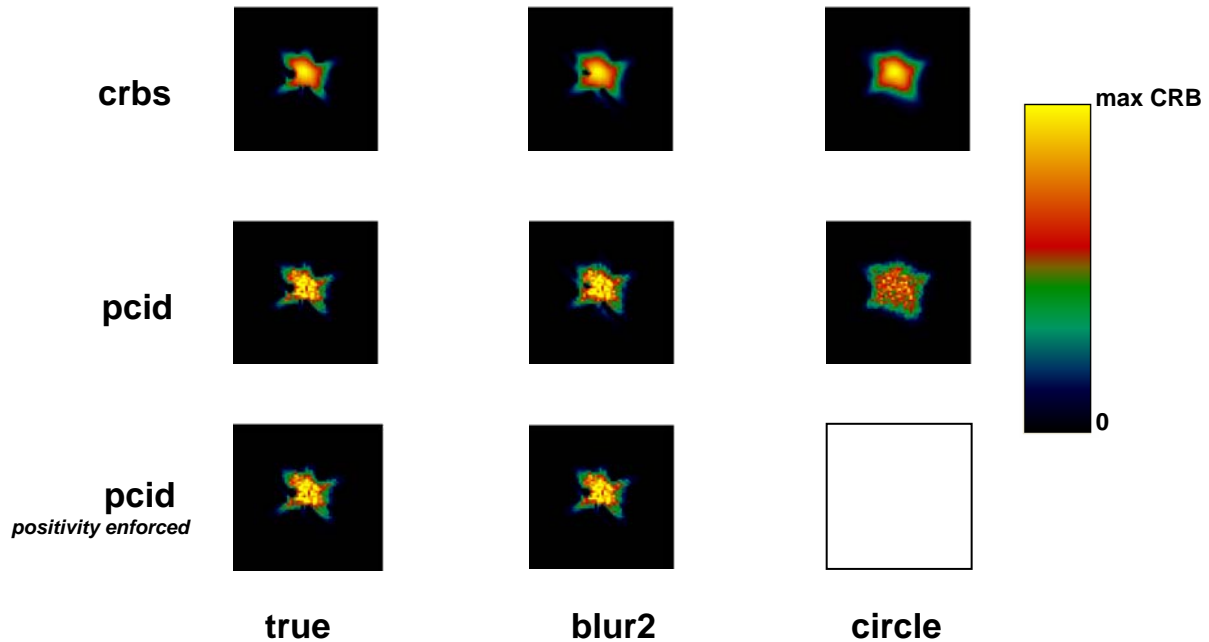


Fig. 3. Photon and read noise case. The first row consists of pixel-by-pixel CRB lower bounds to variance maps. The second and third row consist of PCID sample variance maps and for unconstrained and positivity constrained cases. Support constrained cases are organized by column: perfect or true support, blur2 non-perfect support, and circular support. All PCID variance maps are normalized to the highest value within the associated CRB map located at the top of the column.

4. Conclusions and Future Work

We have employed CRBs as a metric to measure the performance of the PCID algorithm for the cases of a satellite object, ten blurring PSFs, and photon and read noise. Pixel-by-pixel sample variance maps were compared to CRB maps for the case of perfect, tight, but non-perfect, and circular support constraints on the ocnr object. When these support constraints are employed, variances are in numerical and morphological agreement with CRB theory. The PCID sample variances are roughly equal to or slightly higher than the CRBs, however, because PCID reconstructions achieved the global minimum of the associated PCID conjugate gradient search algorithm. PCID sample variances for the positivity enforced case were compared to the CRBs for the unconstrained case. In this case, summed PCID variances dropped below unconstrained CRBs and biases increased, as might be expected. Also, the positivity constraint acts as an object support constraint when loose object supports are employed. In future work, factors that make the PCID algorithm get stuck in local minima will be investigated. Also, the noise reduction benefit of additional frames of data to MFBD algorithms will be investigated. CRB theory indicates that the relative amount of noise reduction per iteration is greater than $1/m$ for the first few frames, where m is frame count, and then shallows out to approximately $1/m$ relative noise reduction per iteration. Sample variances from PCID will be tested for agreement with CRB theory.

The authors wish to thank the Air Force Office of Scientific Research for their financial support of this research.

5. References

- ¹ C.L. Matson and A. Haji, "Cramér-Rao lower bounds for support-constrained and pixel-based multi-frame blind deconvolution," *Proceedings of the SPIE*, vol. 6365 (2006).
- ² M.C. Roggemann and B. Welsh, *Imaging Through Turbulence* (CRC Press, Boca Raton, FL, 1996).
- ³ S.M. Kay, *Fundamentals of Statistical Signal Processing* (Prentice Hall, Upper Saddle River, NJ, 1993).
- ⁴ C.L. Matson, C. C. Beckner, Jr., and K.J. Schulze, "Fundamental limits to noise reduction in images using support - benefits from deconvolution," *Image Reconstruction from Incomplete Data III, SPIE, vol. 5562 (2004)*
- ⁵ C.L. Matson and A. Haji, "Noise reduction in support-constrained multi-frame blind-deconvolution restorations as a function of the number of data frames and the support constraint sizes," *Proceedings of the OSA Topical Workshop on Signal Recovery and Synthesis* (2007)
- ⁶ C. L. Matson and C. C. Beckner, Jr., "Regularization, support constraints, and noise reduction in images – a Cramér-Rao bound analysis," *Proceedings of the OSA Topical Workshop on Signal Recovery and Synthesis* (2005)